Materials & Design 240 (2024) 112834

Contents lists available at ScienceDirect

Materials & Design

journal homepage: www.elsevier.com/locate/matdes

Drop-on-demand metal jetting of pure copper: On the interaction of molten metal with ceramic and metallic substrates

Negar Gilani *, Nesma T. Aboulkhair, Marco Simonelli, Mark East, Richard J.M. Hague

Centre for Additive Manufacturing, Faculty of Engineering, University of Nottingham, Nottingham NG8 1BB, UK

ARTICLE INFO

Keywords:
Additive Manufacturing
Drop-on-demand Metal Jetting
Metal and Ceramic Interface
Copper Microdroplet
MetalJet

ABSTRACT

Copper, renowned for its exceptional electrical and thermal conductivity at a low cost, holds great promise in electronic applications. While additive manufacturing of copper has attracted interest, the exploration of applying Drop-on-demand Metal Jetting (DoD-MJ) to 3D print pure copper remains uncharted. To fill this research gap, we employed an in-house DoD-MJ platform, MetalJet, to generate Cu microdroplets and deposit them onto ceramic and metallic substrates, a first-time achievement in this research context. Our study demonstrates the successful generation of uniform Cu microdroplets, emphasising the pivotal role of oxygen content control in preventing nozzle-level reactions, a factor that can disrupt droplet formation. Both alumina and aluminium nitride substrates exhibited poor wettability with molten Cu droplets, and no interface formed between these surfaces due to thermodynamically unfavourable reactions. Nevertheless, the irregular surface of alumina displayed an interesting capability to enable the adhesion of Cu droplets to the substrate through an interlocking mechanism. Lastly, the electrical resistivity of MetalJet printed pillars was measured as low as $6.75 \times 10^{-8} \Omega m$ without any post-treatment, offering exciting possibilities for applications in 3D electronics.

1. Introduction

Additive manufacturing (AM) has been capturing growing attention across many sectors, with increasing interest in printing functional materials for applications such as functional microelectronics. While nanoparticle-based inkjet printing [1,2] has gained traction as a potential large-scale fabrication method, the incorporation of multiple steps, including ink formulation, nanoparticle synthesis, and post-processing, contributes to the complexity of the process. Furthermore, the issue of higher electrical resistivity compared to the corresponding bulk metal persists. Drop-on-demand Metal Jetting (DoD-MJ) [3] is an emerging AM technology that has shown exciting potential in printing electronics while addressing these complexities. In this approach, individually-controlled droplets of molten metal are directly ejected from a nozzle and deposited onto substrates, demonstrating electrical conductivity in printed traces that closely matches the bulk material [4]. On the material side, surpassed only by Ag, Cu possesses the highest electrical conductivity among metals. It has a high thermal conductivity and has the advantage that it is relatively inexpensive. These attributes collectively make Cu the most intriguing material in the realm of DoD-MJ. However, it has received limited attention in the state of the art, primarily due to the challenges associated with its high melting temperature, oxidation, high surface tension, and high viscosity that pose difficulties for manufacturing.

Selecting a material for a crucible that can withstand temperatures exceeding 1085 °C, the melting point of Cu, without reacting with it while also providing an adequate degree of wetting presents a significant obstacle. The actuation mechanism used to generate droplets must also be compatible with such high temperatures. For instance, piezoelectric materials are unsuitable for operation at elevated temperatures, rendering piezoelectric actuation mechanisms impractical in such conditions [5,6]. While pneumatic actuators have proven effective in high-temperature applications, their usage has primarily been limited to materials such as Ga [7], Sn [8], Sn alloys [9,10], and Al [11]. This limitation arises from the distinctive properties of high-temperature metals such as Cu, including high surface tension ($\gamma_{Cu} = 1312 mNm^{-1}$ vs. $\gamma_{Sn} = 546 mNm^{-1}$) and viscosity ($\mu_{Cu} = 4.02 mPas$ vs. $\mu_{Sn} = 1.85 mPas$). These properties introduce an additional challenge in ejecting individual droplets from a nozzle, necessitating higher energies to overcome interfacial capillary forces.

To date, Zhong et al. [12] have successfully produced Cu droplets ranging from 700 to 1000 μm using a graphite crucible and a pneumatic

* Corresponding author.
E-mail address: negar.gilani@nottingham.ac.uk (N. Gilani).

https://doi.org/10.1016/j.matdes.2024.112834
Received 21 November 2023; Received in revised form 27 February 2024; Accepted 8 March 2024
Available online 11 March 2024

actuator, applying elevated supply pressures as high as 3000 mbar. Moqadam et al. [13] employed an alumina crucible and a pneumatic actuator to generate droplets of AISI 52100 steel with a diameter of approximately 1200 μm, using high-pressure pulses of up to 2945 mbar. Despite these achievements, pneumatic actuators typically operate at low frequencies, usually below 10 Hz, rendering the production rate unsuitable for industrial adoption. Additionally, droplets' velocities consistently remain below 1 m/s. Specifically, for high-melting material, the maximum droplet velocity was reported as 0.086 m/s [12], which is detrimental to the final morphology of droplets upon deposition. Furthermore, the large droplet sizes in these studies are not suitable for the precision and fine resolution required in microelectronic applications. In recent years, Magnetohydrodynamic (MHD) actuators [14,15] have unlocked new possibilities in the production of high-temperature metals, while overcoming the constraints associated with pneumatic actuators. Simonelli et al. [16] demonstrated the MetalJet's capabilities, an MHD actuator-based system, in producing Ag microdroplets ($T > 1000\ ^{\circ}C$) at high frequencies (500 Hz). However, the generation of Cu microdroplets, with their more challenging properties, has not yet been explored to-date.

Identifying a Cu-compatible substrate material with dielectric properties is another challenge in electronic applications. While most polymers provide effective electrical insulation, their inability to withstand high temperatures rules them out as substrate materials in the context of high-temperature DoD-MJ. Hence, ceramics stand as the sole material class suitable for this purpose. In DoD-MJ processes with low Weber numbers bonding mechanisms to the substarte involve: (I) Physical adsorption, where droplets adhere to the substrate through weak Wander Waals forces. (II) Strong metallurgical bonding via substrate melting. (III) Diffusion bonding, forming an intermetallic layer that acts as a joiner [14]. In thermal spraying, mechanical interlocking occurs through localised plastic deformation at interfaces [17]. Notably, mechanical interlocking is achieved only if droplets' speed exceeds a critical impact velocity, typically in the range of 150–900 m/s [18]. However, this is usually not applicable in DoD-MJ processes.

The interaction between metals and ceramics has long intrigued researchers, given its relevance to a wide array of technological products [19]–[21]. However, the bonding between metallic and ion-covalent materials often remains unresolved due to their distinctive properties, the inertness of ceramics and their high melting temperature [22]. The solid-state diffusion bonding between metals and ceramics usually requires high temperature, pressures, prolonged time, and surface preparation to promote mobility and interdiffusion of reacting species across the interfaces [23]. These conditions are not always present in DoD-MJ processes. Liquid-state bonding, on the other hand, is more accessible because the flow of molten metal over the surface eliminates the need for applying high pressures or surface preparations. Additionally, diffusion in the liquid state is orders of magnitude faster than solid-state diffusion [24]. Still, the wettability of the surface by molten material is essential to provide the initial contact between surfaces [25,26]. Yi et al. [27] employed silver coating as a filler to address the issue of Al droplets rebounding from gypsum substrates during a DoD-MJ process. Intriguingly, they observed that the formation of intermetallic compounds, facilitated by Ag dissolving into liquid Al droplets, resulted in strong adhesion, effectively suppressing rebound. Despite the substantial interest in using ceramic substrates for DoD-MJ, the behaviour of molten droplets upon deposition on such substrates, their spreading, and the reactions occurring at the interfaces during and after solidification remain unexplored in the current state of the art.

The aim of this study is to deepen the understanding of the key factors that influence the DoD-MJ of pure Cu, facilitating the manufacturing of 3D Cu structures with micro-resolution, high precision, and superior electrical conductivity. These attributes position the technology as an excellent candidate for microelectronic applications. Firstly, it investigates the generation of molten Cu microdroplets, addressing challenges such as oxidation and nozzle-level reactions. Secondly, this study examines the interaction between Cu microdroplets and commonly used ceramic substrates in electronic applications, namely alumina and aluminium nitride, as well as copper substrates. The investigation employs both experimental and computational approaches to understand the associated challenges, including inter-droplet and droplet-substrate bonding, and microstructure. Finally, the article reports the measurement of electrical conductivity in printed traces and underscores the significance of employing appropriate printing strategies to ensure the consistency of the printed structures.

2. Materials and Methods

The MetalJet platform used in this study is a bespoke DoD-MJ system that generates molten microdroplets through an MHD actuator developed by Canon Production Printing (formerly Océ-Canon) [28]. The system is installed inside a controlled atmosphere glovebox filled with argon that maintains the oxygen level in the processing chamber under 1 ppm. The detailed description of the system can be found in [14,29]. To produce microdroplets, a bipolar actuation waveform was designed, featuring dwell and echo times set at 60 and 15 microseconds, respectively. A comprehensive explanation of the waveform is provided in the Supplementary Material, S1. These waveforms were tailored for copper, ensuring stable jetting, i.e., the generation of a continuous stream of satellite-free droplets, characterised by uniform size and velocity. During the jetting experiment, the real-time measurement and recording of droplet radii and velocities were carried out using a JetXpert drop watcher (ImageXpert Inc., New Hampshire, USA), a stroboscopic camera. Pure copper rods (Grade 5 N) of 5 mm diameter and 20 mm length were acquired from ESPI Metals (Oregon, USA) to be loaded into the cartridges as feedstock. Microdroplets of nearly 84 μm in diameter were ejected at 1140 ℃ with an average velocity of 1.49 m/s at a frequency of 500 Hz.

A Hitatchi TM3030 (Tokyo, Japan) Scanning Electron Microscope (SEM) equipped with a backscatter electron detector operating at 15 keV was used to study the morphology of the produced Cu droplets that were collected in a container 10 cm away from the nozzle. To study the droplet-substrate interfaces and forms of adhesion, individual and adjacent (5 μm overlap) Cu droplets were deposited onto metallic and dielectric substrates. The investigated substrates were alumina Al_2O_3, aluminium nitride AlN, and Cu. The Al_2O_3 and AlN substrates were supplied by CSC Ceramics Ltd (Newport, UK). The tempered Cu sheets of 99.9 % purity were supplied by Advent Research Materials (Oxford, England). All substrates were 20 x 20 x 1 mm in length, width, and thickness, respectively. The surface roughness of these substrates was measured using an optical 3D measurement system, Alicona InfiniteFocusG4 (Alicona Imaging GmbH, Graz, Austria). The average height deviation from the mean value, i.e., Ra, was 0.48 μm, 0.13 μm, and 0.06 μm for Al_2O_3, AlN, and Cu substrates, respectively.

The substrates were heated to 500 ℃ during the printing process to reduce the thermal gradient during the solidification of the droplets and to promote their bonding to the substrates. The distance between the nozzle and the substrates was kept at 1 mm. Focussed Ion Beam (FIB) in FEI Quanta 200 3D Dual Beam (FEI, Hillsboro, Oregon, USA) and Zeiss Crossbeam 550 (Oberkochen, Germany) were used to cross-section the samples. Images were acquired using the Secondary Electron Secondary Ion (SESI) detector operated at 2 kV and 200 pA with a working distance of 5 mm. The solidified microstructures and interfaces of the deposited droplets were also acquired using the FIB-SEM detector. The elemental composition of the interfaces between droplets and substrates was identified via an Energy-Dispersive X-ray (EDX) spectrometer (Oxford Instruments) at a working distance of 5 mm and beam voltage of 10 kV.

A 3D FE (Finite Element) thermal model was used to predict interface temperatures by solving the conduction with general heat convection and radiation boundary conditions. The thermal distribution across the domain complies with Eq. (1), subject to the specified initial and boundary conditions, as well as temperature-dependent material

properties. In Eq. (1), ρ is the density, c_p denotes the specific heat capacity, and k is the thermal conductivity. Comprehensive description of this model is provided in prior studies [14,29]. The geometric properties of the droplet and the contact angle between the droplet and the substrate were determined through experimental measurements using an on-screen image measurement software, IC Measure (the Imaging Source, LLC). The thermo-physical properties of the materials, including density, heat capacity and thermal conductivity, were considered temperature-dependent. A finite temperature range of 2 °C was considered for the solidification of pure Cu (1083–1085 °C), during which the latent heat was 205 kJ/kg.

$$\rho c_p \frac{\partial T}{\partial t} = \frac{\partial}{\partial x}\left(k\frac{\partial T}{\partial x}\right) + \frac{\partial}{\partial y}\left(k\frac{\partial T}{\partial y}\right) + \frac{\partial}{\partial z}\left(k\frac{\partial T}{\partial z}\right) + Q \quad (1)$$

The electrical properties of 10 mm long single- and multiple-droplet pillars were evaluated using a Keithley 2400 source meter and a Keithley 7500 multi-meter. The four-probe method, known as the Kelvin technique, was employed to eliminate contact resistance. A voltage was applied from the two probes at their ends, and the current through the printed line was measured with the change of the voltage drop across the two probes in the middle. Each *I–V* curve was measured three times using both forward and backwards scanning. The derivative of the *I–V* curve revealed the conductivity of the printed line with the precise geometry measured by an optical microscope. To demonstrate the feasibility of using the MetalJet system to fabricate 3D structures, thin walls of various widths (1, 2, 3, and 4 droplets), length of 5 mm, and height of 20 layers were printed on a Cu substrate maintained at 500 °C. Furthermore, a 3D stepped pyramid was manufactured in pure Cu drop-by-drop.

3. Results

3.1. Generation of molten copper microdroplets

The initial and pivotal step in the DoD-MJ processes revolves around the precise ejection of uniform droplets. MetalJet harnesses Lorentz force ($\vec{f}_{MHD} = \vec{J} \times \vec{B}$), where J is the current density and B is the magnetic field, to facilitate droplet ejection. In essence, the current intensity, which governs the electric field, interacts with the permanent magnetic field surrounding the cartridge, thereby exerting control over the formation of droplets. The real-time measurement of droplet radii using the waveform tailored for Cu is depicted in Fig. 1a. At an oxygen content of 5 ppm, the droplet radius exhibited a gradual reduction until the jetting process was prematurely terminated in less than five minutes. This abrupt cessation was due to the chemical reaction between oxygen

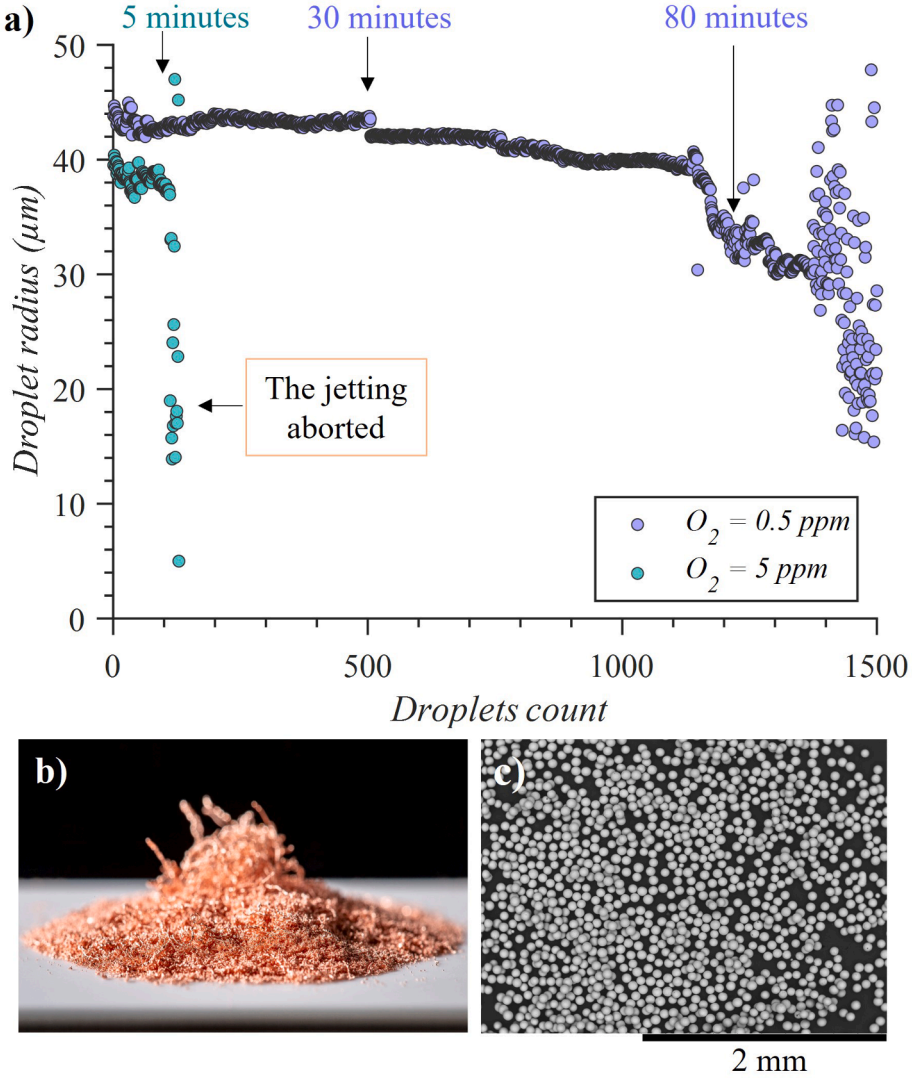

Fig. 1. A) time evolution of ejected droplets radius measured in-situ with a stroboscopic camera at the oxygen contents of 5 and 0.5 ppm, b) Droplets collected in a container placed 10 cm from the nozzle at O_2 = 0.5 ppm, c) SEM image of collected droplets in (b), illustrating the consistent droplet size.

in the process chamber and the molten copper, in conjunction with the inner cartridge coating. This chemical interaction led to the formation of a solid layer enveloping the nozzle, ultimately resulting in its uncontrollable blockage. The mechanism of nozzle blockage is further explained in Section S2 of the Supplementary Material.

Two routes could be adopted to resolve the issue, the first was to change the coating material on the bespoke cartridges used in the MetalJet system, and the second was to enforce tighter control on the atmosphere within the process chamber, i.e., reduce the oxygen content. The latter option was adopted, and a glovebox recirculation system was used, which enabled reducing the oxygen content to approximately 0.5 ppm. The efficiency of controlling the oxygen content in prolonging the duration of jetting is evidenced in Fig. 1a, where a stable stream of droplets with an average radius of 43.3 μm and a standard deviation of 0.41 μm was obtained for thirty minutes. However, the droplet size gradually decreased to 39 μm until the droplet generation was disrupted and eventually aborted in ninety minutes. Droplets ejected under the controlled environment (0.5 ppm) were collected inside a container, positioned 10 cm below the print head (Fig. 1b). The SEM image of the collected droplets in Fig. 1c demonstrates that they are consistent in size and morphology. The spherical morphology of the droplets suggests that during their freefall through the Ar atmosphere, they completely solidified in-flight before impacting the surface of the container. Given the good quality and properties of these particles, it can be argued that the MetalJet technology can also be utilised as a viable route to produce micro- and mono-sized metal powder, expanding its applicability beyond 3D printing of metals. This, however, is out of the scope of the current study and may be the subject of future studies.

The reaction of molten Cu with the limited content of present oxygen (0.5 ppm) inside the glovebox and the ceramic coating inside the cartridge caused the jet stream to deviate from its vertical path, as depicted in Fig. 2a and c. These images were captured at the beginning of the jetting process and after eighty minutes, respectively. Notably, the wettability of molten Cu with the solid layer formed inside the cartridge, stemming from chemical reactions, differs from its wettability with the ceramic coating. This distinction influences the filament extension and the pinch-off process at the orifice level. Since the new layer around the orifice is then non-uniform, the wettability at the orifice levels will become uneven, leading to the formation of a meniscus with various curvatures and, consequently to non-uniform pinch forces at breakup. Eventually, such a distribution causes an inclination in the trajectory of droplets, as schematically demonstrated in Fig. 2e and f. Furthermore, the poorer wettability between the new layer and molten Cu increases the possibility of forming satellite droplets (Fig. 2c) since the ligament is longer and thinner due to a delayed pinch off. Both factors decrease the print quality.

Uniform and stable droplets are crucial for the quality of the structures to be fabricated due to their impact on controlling the landing accuracy of the droplets onto the target substrate as well as the micro- and macroscopic fidelity of the parts. Unstable jetting hinders printing – especially in 3D– as it will be almost impossible to precisely deposit the droplets at their designated locations. The effect of unstable jetting on printing quality is demonstrated in Fig. 2b and d, where a layer of Cu droplets stacked next to each other – with no overlap between the droplets – was printed with the stability monitored over time. The deposition of droplets during the stable jetting was consistent and uniform, within the expected standards of the technology governed by the accuracy of the stage moving under the print head. Conversely, the effects of unstable jetting on deteriorating the quality of the printed layer are evident where the droplets were randomly scattered on the substrate (Fig. 2d), due to the deviation error in deposition and variation in droplet size due to the formation of satellite droplets. This indicates that the reaction inside the nozzle area is non-uniform, leading to the formation of inclusions in some regions while leaving others unaffected. These results underscore the significance of controlling oxidation to prolong jetting stability and maintain uniformity in droplet properties, i.e., size, trajectory, and speed.

3.2. Deposition of copper droplets on an alumina substrate

- Droplet spreading

The interface of a Cu droplet on an Al_2O_3 substrate is shown in Fig. 3a, with the image obtained by peeling the droplet from the substrate using carbon tape. The spreading factor ($S_{max} = D_{max}/D_0$) was only 0.63, and the solidification contact angle was 145°. Numerical simulations indicate that the contact line arrest occurred within 140 μs after deposition, resulting in the droplet freezing in place during the relaxation phase. The cooling profile of individual Cu droplets on Al_2O_3 substrates is illustrated in Fig. S3 in the Supplementary Material. The solidification contact angle exceeding 90° during the relaxation phase suggests that Cu was unable to effectively wet the Al_2O_3 substrate. Correspondingly, prior research has reported that the contact angle of pure copper on Al_2O_3 is approximately 128° at 1150 °C [25]. It is

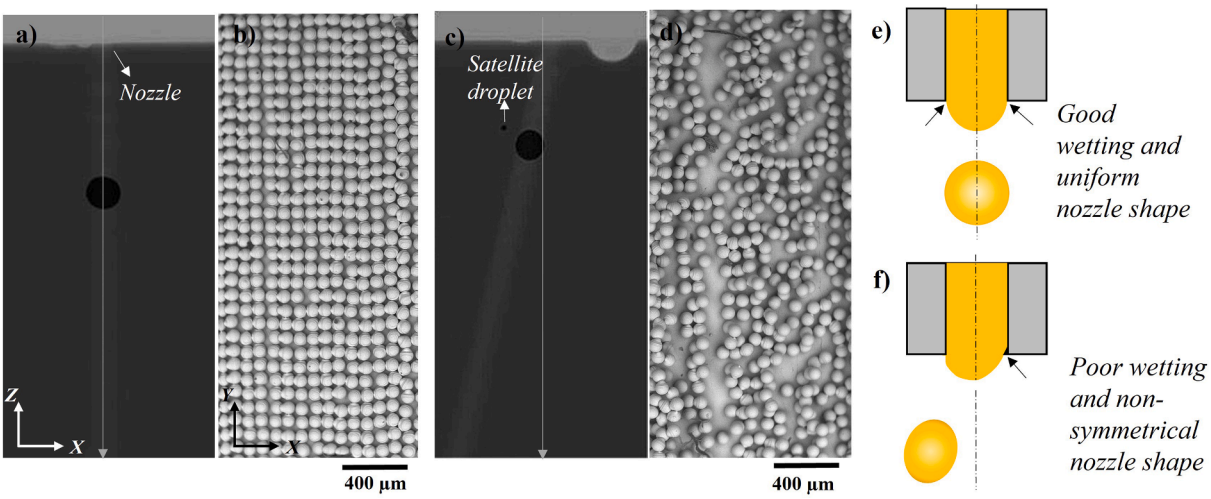

Fig. 2. A) perpendicular trajectory of the jet stream to the nozzle plate during the first eighty minutes, b) sem image of droplets deposited onto a cu substrate at 500 °C, demonstrating precise voxel-by-voxel deposition as a result of stable jetting, c) Deviation from the normal trajectory after eighty minutes of jetting due to the reaction of molten Cu with oxygen and coating inside the cartridge, d) Effects of jetting instability on printing accuracy. Schematic representation of wettability and uniformity effects at the orifice level on the generation of e) Vertical stream and uniform droplets, and f) Inclination of droplet trajectory.

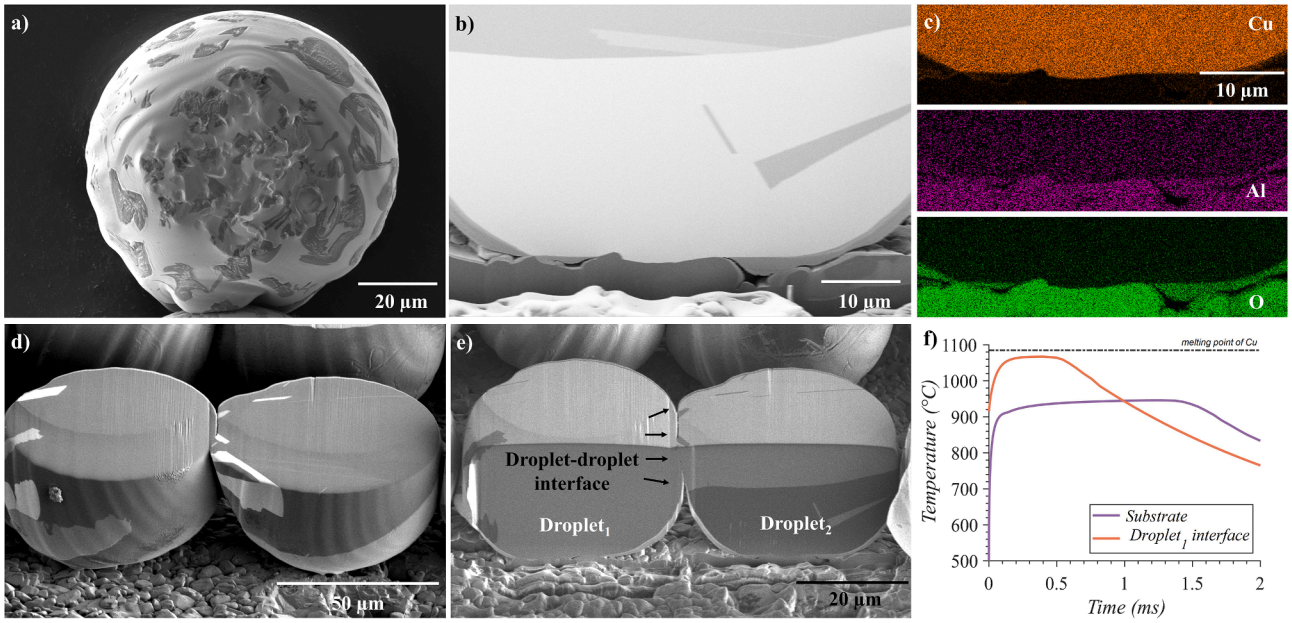

Fig. 3. A) interface of an individual cu droplet with Al_2O_3 substrate, captured by peeling and mounting droplets on a C tape. b) Cross-section of Cu droplets with Al_2O_3 substrate, revealing the absence of fusion bonding at the interface. c) EDX analysis of the cross-section, illustrating no diffusion at the interface. d) Cross-sectional view displaying the interface between the droplets and the grain structure. e) Cross-section displaying inter-droplet and droplet-substrate interfaces. f) Temperature evolution at the interface of previously deposited droplets during the deposition of new droplets, along with the temperature evolution of substrate during the deposition of a single droplet.

recognised that the primary requirement for successful printing on a substrate is establishing intimate atomic contact at the interface between droplets and substrates, facilitated by Van der Waals attraction forces. In such physical bonding, no mass transfer occurs across the interface, and the wettability of the substrate with the molten droplet determines whether the droplet adheres to the surface or rebounds. Due to poor wettability and a slow solidification rate resulting from the low thermal conductivity of Al_2O_3, it was expected that droplets would bounce off from the substrate in a non-wetting condition [14]. However, during printing, it was observed that the majority of droplets adhered to the substrate, with only a few exhibiting random rebounding behaviour. The observed cavities at the interface of the droplet in Fig. 3a correspond to the surface irregularities on the Al_2O_3 substrate.

The average maximum profile peak height, R_{pm}, obtained from surface roughness measurements, was 0.8 µm on the Al_2O_3 substrate, corresponding to the cavity size with approximately similar depth as observed in FIB-SEM images (Fig. 3a–c). R_{pm} is calculated as the average of successive R_{pi} values through the evaluation length. In this context, the maximum profile peak height, R_p, denotes the distance between the highest point of the profile and the mean line over the evaluation length. These irregularities are anticipated to have functioned as pinning sites, resulting in localised deformations before solidification occurred. Indeed, the rough substrate features, acting as micro-capillary bridges, facilitated interlocking within these grooves, promoting droplet adhesion to the substrate. Importantly, the interlocking mechanism in this case differs from the mechanical interlocking observed in thermal spraying, where plastic deformation causes bonding to the substrate. It is worth noting that the liquid Cu could not infiltrate the pores on the surface of the Al_2O_3 substrate due to its inability to overcome the pressure difference induced by capillary action, as derived from Eq. (2) [30].

$$\Delta P = 2\gamma cos\theta / r \tag{2}$$

Where θ represents the contact angle and γ denotes surface tension. According to Eq. (1), a pressure of 0.5 MPa is necessary for the liquid metal to infiltrate the cavities in the Al_2O_3 substrate. Due to the small size of droplets, the gravitational forces, equal to 4.2×10^{-6} MPa, are significantly lower than the required pressure. This explains why the pores were not filled with the molten metal. It is important to note that during the FIB milling process, the material sputtered from the substrate has occupied the pores in the substrate (Fig. 3b), and this should not be mistaken for molten metal filling these gaps. The EDX map shown in Fig. 3c provides clear evidence of this phenomenon.

- Bonding at the interfaces

The second condition required for successful printing on a substrate is ensuring adequate bonding with the substrate. Melting of materials with ionic bond configuration, such as most ceramics, involves breaking the ionic bonds and occurs at high temperatures. Alumina, being a highly ionic material with a melting point of 2045 °C, does not offer a feasible option for forming a strong bond with Cu through substrate melting. According to the computational results in Fig. 3f, the substrate temperature reaches 900 °C during the droplet deposition, significantly below the melting point of Al_2O_3. The alternative approach is establishing a stable chemical thermodynamic equilibrium at the interface. This results in a strong bonding in which there is mass transfer across the interface, such as chemical reaction and diffusion. One possible solution for printing on ceramics that are inherently non-wettable by metals is to promote reactive wetting at the interface. In reactive wetting, the chemical reactions reduce the free energy, consequently significantly reducing interfacial tension. According to previous studies, the reaction between Cu and Al_2O_3 is not thermodynamically favourable in the absence of O_2 [22]. A layer of copper aluminates, $CuAlO_2$, can only be formed through the reaction between Cu_2O and Al_2O_3 (Eq. (3) since it is thermodynamically favourable, as indicated in Eq. (4) [25].

$$Cu_2O(s) + Al_2O_3 \rightarrow 2CuAlO_2(s) \tag{3}$$

$$\Delta G^{\circ} = -23740 + 10.43\,T\,(J/mol) \text{ for } 1300\,K < T < 1500\,K \tag{4}$$

$CuAlO_2$ can only be formed if there is a supply of free O_2 to react with molten Cu and form Cu_2O (Eq. (5). Even though the diffusion rate of oxygen into molten copper is very rapid, with a diffusion coefficient of $6.2 \times 10^{-9} m^2/s$ at 1100 °C [22], the phase diagram of Cu and O_2

indicates that an ample oxygen supply is necessary to reach the equilibrium content of 33 %.

$$2Cu(l) + \frac{1}{2}O_2(g) \rightarrow Cu_2O(s) \quad (5)$$

The absence of O_2 during the in-flight stage and at deposition prevents the formation of an interlayer that could have ensured a strong bond between the ceramic substrate and the Cu droplets. This observation was supported by the EDX map presented in Fig. 3c, where it is apparent that the interface between Cu and Al_2O_3 remains distinct, with no new interfaces formed between them. The presence of O_2 could also be beneficial in improving the wettability between Cu and Al_2O_3. It has been shown that the Cu-O system can reactively wet and adhere to Al_2O_3. In these cases, the Al_2O_3 dissociates, and the dissolution of Al and O_2 in the moving interface could decrease the contact angle to as low as 12°, and increase the work of adhesion to 1340 mJ/m2 [20]. The work of adhesion in the current system can be obtained from Eq. (6), which is equal to 503.5 mJ/m^2.

$$W_a = \gamma(1 + cos\theta) \quad (6)$$

The top section of two sequentially deposited droplets was removed through FIB milling to investigate the bonding at their interfaces (Fig. 3d–e). An evident line separating the two droplets at the interface suggests that no remelting occurred at the interface. The computational results in Fig. 3f demonstrate that the deposition of the second droplet raises the temperature of the previously deposited droplet at the interface up to 1050 °C, which remains below the melting point of Cu. Since these high temperatures were sustained for a brief period, less than a millisecond in this case, the conditions necessary for necking and sintering between the droplets were not met, aligning with the experimental observations. Moreover, large inter-droplet pores are evident at the lower section of droplets in Fig. 3e, representing a common defect in DoD-MJ processes [16,31]. This phenomenon arises from inadequate wettability between the Al_2O_3 substrate and Cu droplets, exacerbated by the elevated surface tension of Cu, thereby resulting in enlarged pores. Irrespective of solidification kinetics and spreading dynamics, such pore formation is anticipated when the substrate is not wettable by molten droplets.

An intriguing aspect observed in Fig. 3d–e is the formation of coarse grains in the droplets. The microstructure of the first droplet primarily comprises a single grain, while the second droplet mainly exhibits two coarse grains. One was formed in the contact area with the previously deposited droplet, and the other emerged from the interface with the substrate. The formation of this distinctive grain structure is attributed to the low thermal conductivity of the Al_2O_3 substrate, leading to a slow solidification rate in the droplets.

3.3. Deposition of copper droplets on an aluminium nitride substrate

- Droplet spreading

Aluminium nitride's outstanding thermal conductivity promotes efficient heat dissipation, while its excellent electrical insulation minimises signal loss and interference. These attributes make it an appealing choice as a substrate material for electronic applications. Consequently, AlN was chosen as the second ceramic substrate for this study. Fig. 4a, presents measurements of the contact area of a single Cu droplet on an AlN substrate. The analysis revealed a spreading factor of 0.69 and a solidification contact angle of 124°. It is important to note that the equilibrium contact angle for this system is 155° at 1150 °C [32], underscoring AlN's profound non-wettability with molten Cu. The smaller observed solidification contact angle can be attributed to the contact line being arrested during the spreading phase, occurring more rapidly than the completion of the spreading cycle.

Computational results informed that the droplets pinned to the substrate in less than 53 μs. The cooling profile of individual Cu droplets on AlN substrates is depicted in Fig. S3 in the Supplementary Material. This relatively rapid solidification originates from the superior thermal conductivity of AlN compared to Al_2O_3. During the printing process, the challenge of droplets randomly rebounding off the substrate was encountered, making it difficult to create continuous traces or straight lines. This issue can be ascribed to the substrate's inadequate wettability

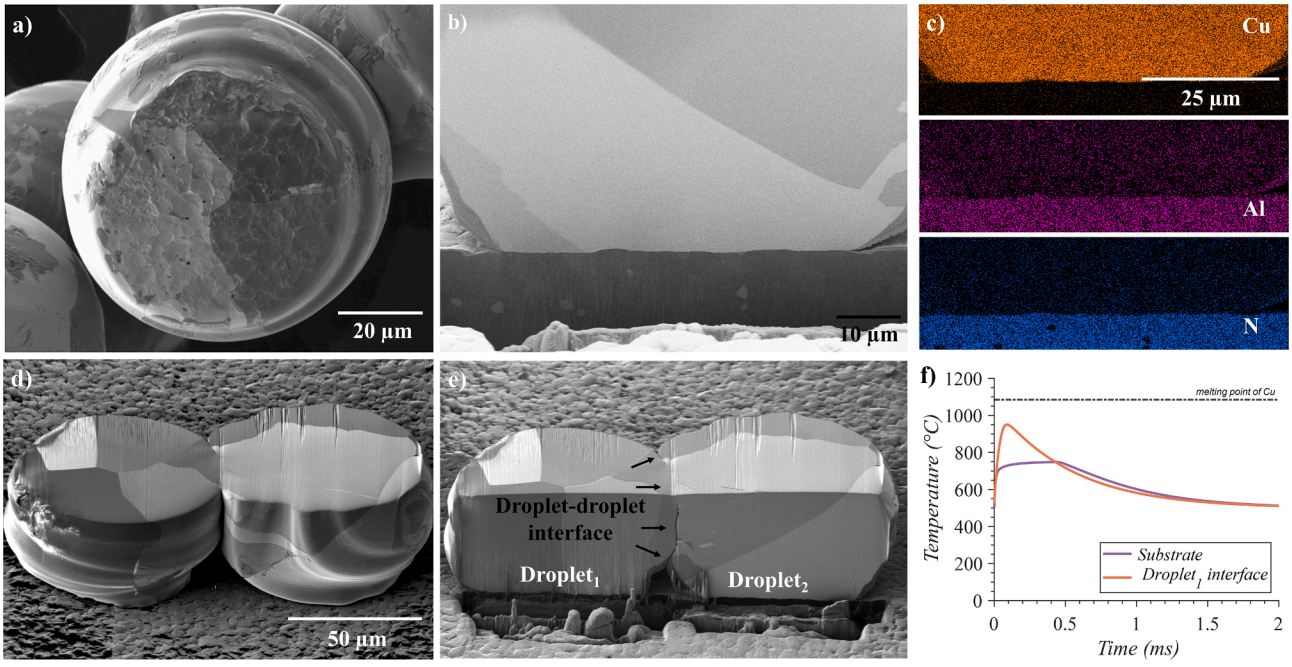

Fig. 4. A) interface of an individual cu droplet with AlN substrate captured by peeling and mounting droplets on a C tape. b) Cross-section of Cu droplets with AlN substrate illustrating the lack of fusion bonding at the interface. c) EDX analysis of the cross-section, showing no diffusion at the interface. d) Cross-sectional view with the interface between the droplets and the grain structure. e) Cross-section displaying inter-droplet and droplet-substrate interfaces. f) Temperature evolution at the interface of previously deposited droplets during the deposition of new droplets, the temperature evolution of substrate during the deposition of a single droplet.

by molten Cu. In this case, the substrate surface is smoother, reducing the likelihood of interlocking. According to Eq. (2), a pressure of 0.8 MPa is required to overcome the capillary forces and infiltrate the pores, which is much higher than the pressure available in the system due to the gravitational forces.

- Bonding at the interfaces

The FIB-SEM image and the EDX map in Fig. 4b–c reveal that no interface formed when the molten Cu came into contact with the AlN substrate. This can be attributed to the fact that the reaction between Cu and AlN is thermodynamically unfavourable. Intriguingly, in this system, the reaction can only occur if sufficient oxygen is present to form an initial layer of CuO_2, which subsequently reacts with AlN according to Eq. (7). In accordance with Eq. (8), not only is this reaction thermodynamically favourable, but AlN is also wettable by CuO_2, resulting in contact angles as low as 30° [32].

$$CuO_2 + \frac{2}{3}AlN \rightarrow \frac{1}{3}AlO_2 + 2\,Cu + \frac{1}{3}N_2 \tag{7}$$

$$\Delta G^{\circ} = -178198 - 37.1\,T\,(J/mol) \tag{8}$$

It is noteworthy that the melting point of AlN stands at 2200 °C. As per the computational results in Fig. 4f, the substrate's temperature reaches only 750 °C during the deposition of droplets, which remains substantially below the threshold required for bonding through fusion. In this context, the work of adhesion is calculated to be 122.7 mJ/m^2, which is four times lower than that of Cu and Al_2O_3. This implies that the droplets are more likely to detach from the substrate in the current system.

As depicted in Fig. 4d–e, upon removing the top and side sections of two sequentially deposited droplets with FIB, a distinct interfacial line between these droplets became evident, confirming the absence of remelting at the interface. Furthermore, the computational results, as presented in Fig. 4f, corroborated these experimental findings by predicting that during the deposition of the second droplet, the interfacial temperature of the first droplet would not attain the melting point of Cu. An intriguing observation from Fig. 4d–e lies in the contrasting grain structures of $droplet_1$ and $droplet_2$. In the former, large columnar grains predominantly grew from the interface with the substrate, while in the latter, grains primarily nucleated and grew from the interface with the first droplet. This behaviour can be attributed to the higher thermal conductivity of Cu at 500 °C (366 W/m·K) compared to AlN (55 W/m·K). Consequently, in the second droplet, grain growth occurred in a competitive interplay between heat conduction through the interface with the previously deposited Cu droplet and the AlN substrate, with the former exerting a more dominant influence.

3.4. Deposition of copper droplets on a copper substrate

- Droplet spreading

To investigate the behaviour of molten Cu droplets on an inherently wettable substrate, Cu substrates, conducive to potential metallurgical bonding, were selected. Printed droplets were detached from the substrate using a carbon tape, and their interfacial characteristics were investigated, as depicted in Fig. 5a. What is particularly noteworthy in this figure is the formation of a polycrystalline structure at the interface,

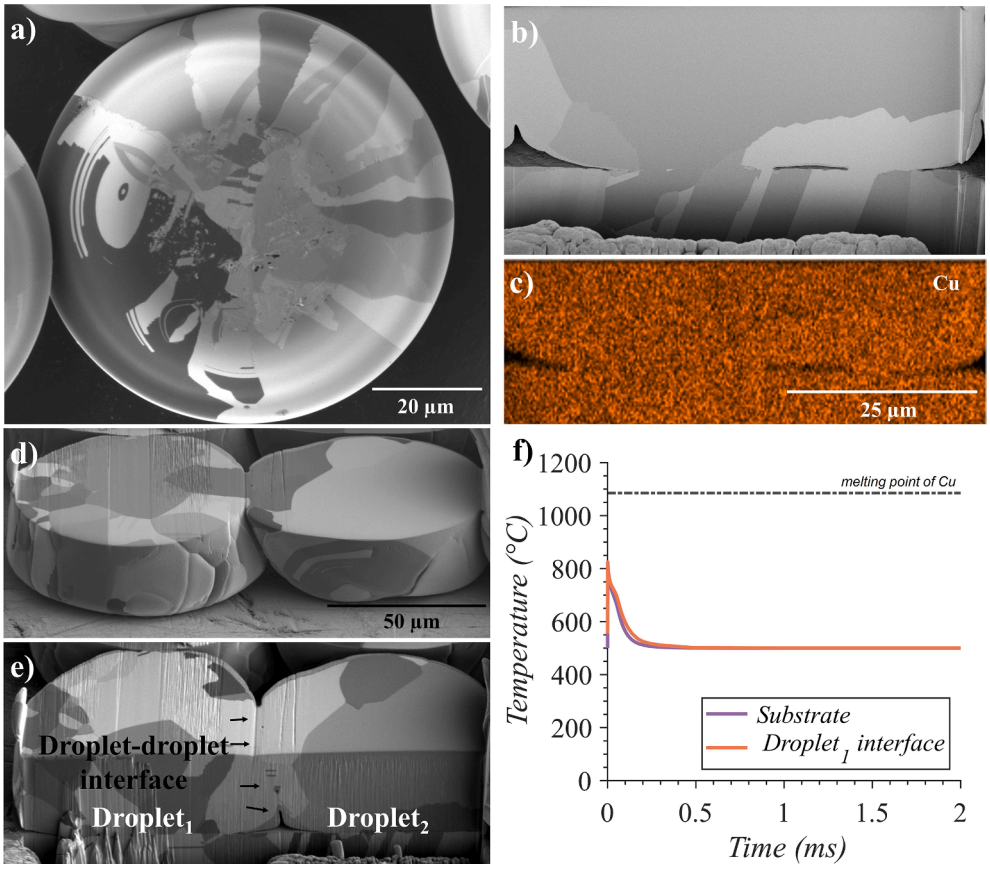

Fig. 5. A) the interface between an individual cu droplet and a cu substrate, captured by peeling and mounting droplets on a c tape. b) cross-section of cu droplets with a cu substrate, revealing a lack of fusion bonding at the interface. c) edx analysis of the cross-section, displaying no diffusion at the interface. d-e) cross-sectional view with the interface between the droplets and the grain structure. f) temperature evolution at the interface of previously deposited droplets during the deposition of new droplets and the temperature evolution of substrate during the deposition of a single droplet.

characterised by smaller grains at the droplet's centre and larger grains at its edges. This observation stands in contrast to the characteristics of Cu droplet interfaces on ceramic substrates. This disparity is primarily attributed to the difference in thermal conductivity between the Cu substrate (366 W/m.K) and ceramic substrates (10–55 W/m.K) at 500 °C. As a result, a higher solidification rate was experienced by Cu droplets deposited on Cu substrates, leading to the formation of the observed polycrystalline structure at the interface. In the present case, the spreading factor measured 0.78, while the solidification contact angle was 85°. It is to be noted that under ideal circumstances, the Cu substrate should exhibit wetting of the Cu droplet, thereby yielding a smaller contact angle. However, in this case, the contact line was arrested almost instantaneously upon droplet deposition, i.e., during the kinematic phase, halting the further spreading of the droplet. Furthermore, the Cu substrate's finely polished surface led to the smoother interfaces of the droplets compared to those deposited on ceramic substrates.

- Bonding at the interfaces:

The interfacial line separating the droplet from the substrate became visible after FIB milling, as evidenced in Fig. 5b–c, indicating an absence of substrate melting, and consequent lack of metallurgical bonding between the droplet and the substrate. The lack of melting can be attributed to insufficient thermal energy in the droplet by the time it impacts the substrate, as supported by computational results presented in Fig. 5f. Notably, during the droplet deposition, the substrate temperature reached a maximum of 760 °C, which remains below its melting point. Furthermore, as depicted in Fig. 5b, there is no indication of epitaxial growth at the interface. Consequently, the droplets adhered to the substrate through weak van der Waals forces, consistent with prior investigation [29]. The work of adhesion in this case was equal to 2620 mJ/m^2, a value five times greater than that observed in the Cu and Al_2O_3 system, suggesting that droplets are less easily to be peeled off from the substrate. It is expected that elevating the initial temperatures of both the substrate and droplet would enhance the likelihood of establishing a robust metallurgical bond through substrate melting. This prospect merits exploration in future investigations.

Upon the removal of the caps of the droplets using FIB-milling (Fig. 5d), it can mistakenly be perceived that some bonding may have occurred between the droplets due to grains coalescing at the interface. However, Electron BackScatter Diffraction (EBSD) mapping of the interface in an earlier study by the authors [29] has confirmed that this is not the case since the crystallographic orientation of the grains at the interface showed a clear partitioning between the adjacent droplets. The reason behind this illusion created by the ion beam is attributed to the operational concept of the ion beam and how it collected image data from the specimen. The FIB was then used to mill away material in the plane perpendicular to the revealed cross-section, as depicted in Fig. 5e, the lack of droplet remelting is evident in the cross-sectioned area, which is marked with black arrows. The computational results revealed that the interface of the first droplet is heated only to 820 °C, yet below the melting point of Cu, which agrees with the experimental observations.

Another interesting point in Fig. 5d–e is the difference between the microstructure of the first and second droplets. As $droplet_1$ landed on the substrate, it dissipated its energy predominantly into the Cu substrate, which has a high thermal conductivity. Therefore, a faster solidification rate is enforced, which promotes the formation of a finer grain structure when compared to the droplets deposited on AlN and Al_2O_3 substrates. Conversely, the following droplets experienced a faster solidification rate, as the following droplets have more contact area (with the proceeding droplets and the substrate) that can be utilised for energy dissipation during the droplets' solidification. This scenario only holds when sufficient overlap is ensured between the adjacent droplets via stable jetting. Columnar grains were seen originating at the centre point of the droplet-substrate interface and then growing aligned with the direction of the thermal gradient towards the periphery of the droplet.

3.5. Electrical resistivity of printed structure

Four-point probe measurements were conducted to determine the electrical resistivity of pillars of singular (Fig. 6a–b) and multiple (Fig. 6c) droplets printed through the MetalJet platform. These measurements provided the resistance values based on the Ohm's law, $R = \frac{U}{I}$, and the resistivity was obtained as follow:

$$\rho = \frac{RA}{L} \tag{9}$$

where A represents the cross-sectional area, and L represents the length of the pillars, obtained from the SEM images and optical microscopy, respectively. The four-point measurements in Fig. 6c reveal linear and symmetrical I-V characteristics for both cases, indicating that the MetalJet-printed pillars exhibit the desired Ohmic behaviour. The electrical resistivity of the pillars formed by a single droplet was $\rho = 8.48 \times 10^{-8} \Omega m$, while the resistivity of pillars manufactured by multiple droplets was $\rho = 6.75 \times 10^{-8} \Omega m$. It is evident that by increasing the diameter of the pillar, achieved by printing multiple droplets, the resistivity decreases. This reduction can be attributed to the formation of a more continuous pathway for charge transport.

In both cases, the low resistivity of Cu pillars printed by MetalJet surpasses that of previous additively manufactured Cu traces by a significant margin. Recent Cu NP inkjet-printed traces, even after laser sintering, have achieved a resistivity of $1.1 \times 10^{-7} \Omega m$ [33], which still remains 1.6 times higher than the values obtained here (without any post-processing). For reference, the resistivity of bulk Cu is reported to be $1.77 \times 10^{-8} \Omega m$, indicating that the MetalJet samples, even without heat treatment to improve consolidation, exhibit only 3.8 times higher resistance than the bulk material. It should be noted that despite being held together by van der Waals forces, the lack of metallurgical bonding at the interfaces, as discussed in previous sections, suggests that each droplet can be considered a distinct solid body. When an electric current flows through the interface of two contacting solids, it induces a change in electric potential, known as electrical contact resistance. This is primarily due to asperities in contact regions, and resistance can increase with higher surface roughness or oxidation. In our study, controlled deposition in an environment with 0.5 ppm oxygen prevents droplet oxidation. Moreover, the droplets are in perfect contact since they are deposited in liquid form. Both factors contribute to low resistivity in printed pillars.

It is anticipated that by enhancing the metallurgical bonding in the samples, the resistivity would decrease even further. Furthermore, it is essential to consider that the charge carrier mobility is strongly dependent on crystallinity and micro-nano structure. High-angle grain boundaries are known to be the primary lattice imperfections that contribute to electron scattering, thereby reducing conductivity [34]. As discussed in our previous research [29], despite the lack of remelting, low-angle grain boundaries at the interface between Cu droplets could be obtained, which explains the low resistivity in the printed pillars.

3.6. Copper 3D printing using MetalJet

- Printing strategies

In the realm of 3D printing using DoD-MJ technology, achieving desired physical and mechanical properties entails a thorough consideration of both metallurgical and geometrical factors. While previous sections covered metallurgical aspects, the following discussion delves into critical geometrical factors, encompassing printing parameters and strategies. To this end, single tracks, i.e., individual lines, and layers, i.e., overlapping lines, were printed using variable droplet spacings. With the

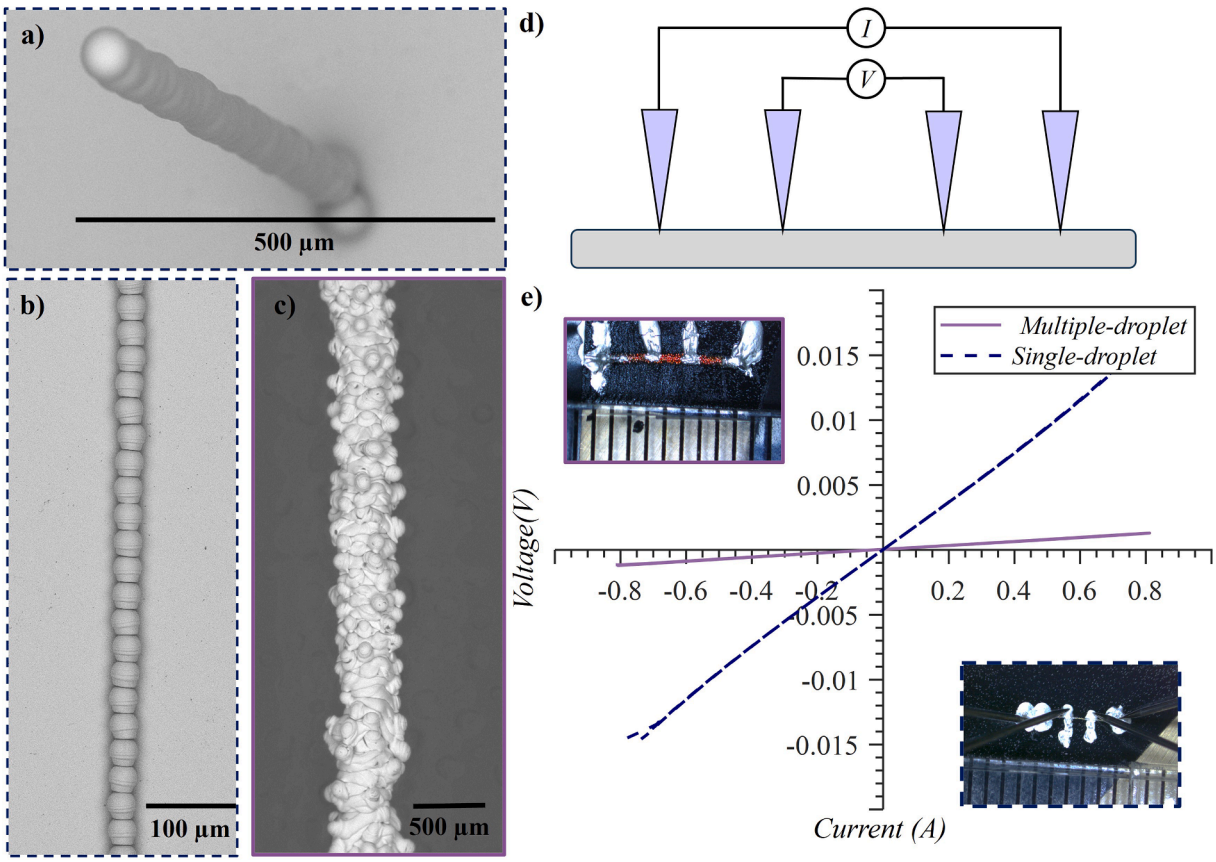

Fig. 6. A) sem image of pillars manufactured by individual cu droplets on a cu substrate, b) corresponding image of the pillar in (a) placed horizontally on a substrate, c) sem image of a cu pillar manufactured by multiple droplets, placed on a carbon tape, d) schematic representation of four-point probe measurements, d) four-point terminal current–voltage (i–v) characteristics of pillars shown in (b) and (c), along with optical microscopy images of the pillars.

droplet size being 84 µm in diameter on average, a droplet spacing of 79 µm translated into an overlap of 5 µm between the droplets. The SEM image in Fig. 7a–c demonstrates the overlap was insufficient to provide adequate contact area between the droplets. A droplet spacing of 74 µm, on the other hand, translated into an overlap of 10 µm, yielding better contact between the droplets (Fig. 7d–f). Nevertheless, it was evident that the droplets did not fully consolidate to form a void-free layer, as evidenced by the gaps between the stacked droplets in both cases.

This finding is similar to results published by Simonelli et al. [16] in an earlier study on using MetalJet to print 3D structures in Ag. Despite the significant difference between the architecture of the system used in the current study and that of Simonelli et al., the lack of bonding and consolidation between the droplets remained an issue. Approaches to enhance the droplets' bonding and overall part consolidation include (1)

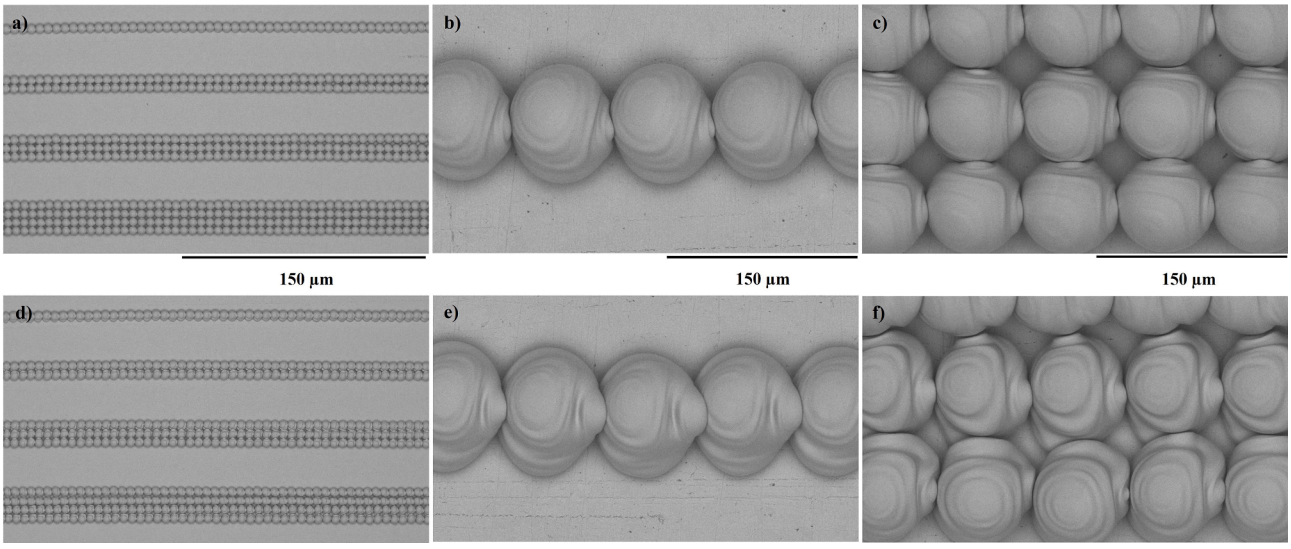

Fig. 7. Single tracks and layers of Cu with a-d droplet spacing of 79 µm and e-h) spacing of 74 µm, highlighting the significance of droplet spacing in enhancing the density of printed structures.

Exploring droplet deposition strategies, such as the staggered droplets approach, (2) increasing the substrate temperature beyond 500 °C, (3) increasing the jetting temperature to increase the droplet temperature, (4) increasing the jetting frequency, and (5) implementing post-printing heat treatments for sintering. Methods (1) and (5) have demonstrated promising potential for Ag [16], and Methods (2) and (3) have demonstrated to be efficient for Sn [14]. The applicability of these methods to 3D print Cu structures will be the subject of future work.

- MetalJet printed structures in copper

The capability of the MetalJet technology to print 3D structures in Cu is demonstrated in Fig. 8. Cu walls of variable thickness, ranging from 84 μm to 400 μm, were successfully printed onto a Cu substrate (Fig. 8a). Additionally, a stepped micro-pyramid was also printed on a Cu substrate (Fig. 8b), serving as another demonstration of the system's capability in printing freeform 3D parts one drop at a time. It is evident that the drop-on-demand deposition of pure Cu to build 3D structures with a resolution of less than tens of micrometres is feasible through this technology. These objects have been shown to exhibit electrical conductivity comparable to that of the pure material. Future work will focus on overcoming jetting issues to extend the usage duration of single cartridges, incorporating the recommendations in this article to enable printing on dielectric substrates, and enhancing the level of inter-droplet bonding.

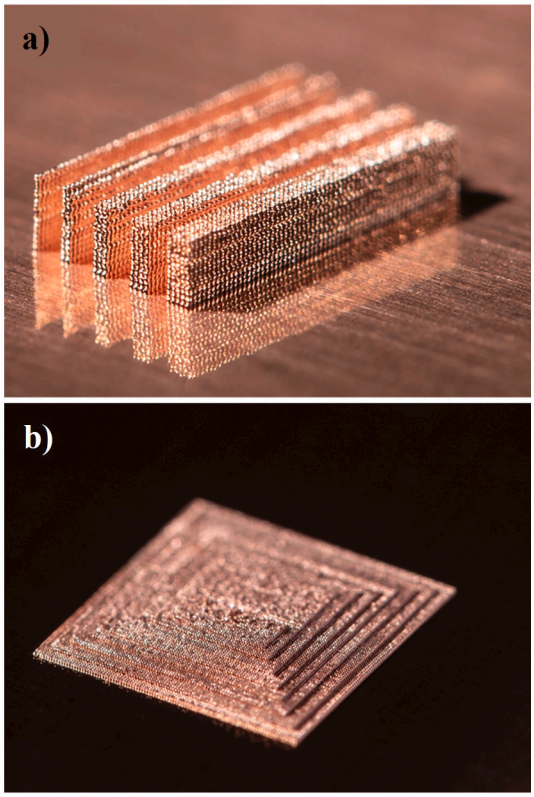

Fig. 8. A) micro-walls of cu with varying thicknesses on a cu substrate, b) micro-stepped pyramid of cu on a cu substrate, manufactured through the metaljet platform.

4. Conclusions

In this study, uniform-sized Cu microdroplets were successfully generated using a novel MHD-based DoD-MJ platform. These droplets were deposited onto Al_2O_3, AlN, and Cu substrates, and the interactions and bonding at their interfaces were investigated. Despite the poor wettability of both ceramic substrates with Cu, the deposition of droplets on the Al_2O_3 substrate was possible due to its surface heterogeneities, which acted as micro-capillary bridges during spreading, and pinned droplets to the substrate as they solidified. It was observed that maintaining oxygen content below 0.5 ppm in the printing chamber prevented the formation of interfaces between Cu droplets and ceramic substrates. Furthermore, computational results indicated that substrate melting conditions were not met when printing on Cu substrates. Nevertheless, the droplets adhered to substrates through weak van der Waals forces. The significant outcome of this research is the low electrical resistivity of the printed pillars, achieved without the application of heat treatment. Despite the absence of remelting and epitaxial growth at the interfaces between droplets, the measured electrical resistivity was only 3.8 times higher than that of the bulk material. This finding offers significant potential for the integration of the MetalJet technology in the electronics industry.

CRediT authorship contribution statement

Negar Gilani: Writing – original draft, Methodology, Investigation, Formal analysis. **Nesma T. Aboulkhair:** Writing – original draft, Investigation, Funding acquisition, Formal analysis, Conceptualization. **Marco Simonelli:** Writing – review & editing. **Mark East:** Resources. **Richard J.M. Hague:** Writing – review & editing, Project administration, Funding acquisition.

Declaration of competing interest

The authors declare that they have no known competing financial interests or personal relationships that could have appeared to influence the work reported in this paper.

Data availability

Data will be made available on request.

Acknowledgements

The authors are grateful to EPSRC for funding the MetalJet printing activity through grant reference (EP/P031684/1). The authors are also grateful for the funding provided by the University of Nottingham's Anne McLaren Fellowship and Nottingham Research Fellowship. The authors would like to thank colleagues at Canon Production Printing, Venlo, The Netherlands, for ongoing technical support with regards to the printing platform. Thanks to nmRC forgranting access to the facilities, and to Dr Christopher Parmenter and Dr Nigel Neate for their training on FIB-SEM and EDX. Thanks to Dr Feiran Wang for assistance in electrical conductivity measurements.

Appendix A. Supplementary data

Supplementary data to this article can be found online at https://doi.org/10.1016/j.matdes.2024.112834.

References

[1] J. Im, et al., Functionalized Gold Nanoparticles with a Cohesion Enhancer for Robust Flexible Electrodes, ACS Appl. Nano Mater 2022 (2022) 6716, https://doi.org/10.1021/acsanm.2c00742.

[2] G. Rivers, et al., Stable large area drop-on-demand deposition of a conductive polymer ink for 3D-printed electronics, enabled by bio-renewable co-solvents, Addit. Manuf. 66 (Mar. 2023) 103452, https://doi.org/10.1016/j.addma.2023.103452.

[3] N. Gilani, A. Foerster, and N. T. Aboulkhair, "Material Jetting," pp. 371–387, 2023, doi: 10.1007/978-3-031-20752-5_23.

[4] M. Meda, P. Mehta, C. Mahajan, B. Kahn, D. Cormier, Magnetohydrodynamic liquid metal droplet jetting of highly conductive electronic traces, Flex. Print. Electron 6 (2021) 35002, https://doi.org/10.1088/2058-8585/ac0fee.

[5] T.Y. Ansell, Current Status of Liquid Metal Printing, J. Manuf. Mater. Process (2021), https://doi.org/10.3390/jmmp5020031.

[6] H. Yi, L. Qi, J. Luo, D. Zhang, H. Li, X. Hou, Effect of the surface morphology of solidified droplet on remelting between neighboring aluminum droplets, Int J Mach Tool Manu 130–131 (August) (2018) 1–11, https://doi.org/10.1016/j.ijmachtools.2018.03.006.

[7] S. Gao, et al., Stabilization formation characterization of metal single droplet by pneumatic drop-on-demand, Phys. Fluids 34 (12) (Dec. 2022) 122010, https://doi.org/10.1063/5.0129467/2843777.

[8] V.A. Beck, et al., A combined numerical and experimental study to elucidate primary breakup dynamics in liquid metal droplet-on-demand printing, Phys. Fluids 32 (2020) 112020, https://doi.org/10.1063/5.0029438.

[9] R. Zamora, F. Faura, J. Hernández, J. López, Volume-conservative modeling of structures manufactured by molten drop-on-drop deposition, Mater. Des. 221 (Sep. 2022) 110970, https://doi.org/10.1016/J.MATDES.2022.110970.

[10] H. Sohn, D.Y. Yang, Drop-on-demand deposition of superheated metal droplets for selective infiltration manufacturing, Mater. Sci. Eng. A 392 (1–2) (Feb. 2005) 415–421, https://doi.org/10.1016/J.MSEA.2004.09.049.

[11] N.N. Watkins, E.S. Elton, P.H. Paul, J.R. Jeffries, A.J. Pascall, Experimentally probing the extremes of droplet-on-demand printability via liquid metals, Phys. Fluids 33 (2021) 121301, https://doi.org/10.1063/5.0076594.

[12] S.Y. Zhong, L.H. Qi, J. Luo, H.S. Zuo, X.H. Hou, H.J. Li, Effect of process parameters on copper droplet ejecting by pneumatic drop-on-demand technology, J. Mater. Process. Technol. 214 (12) (2014) 3089–3097, https://doi.org/10.1016/J.JMATPROTEC.2014.07.012.

[13] S.I. Moqadam, L. Mädler, N. Ellendt, A High Temperature Drop-On-Demand Droplet Generator for Metallic Melts, Micromachines 10 (2019), https://doi.org/10.3390/mi10070477.

[14] N. Gilani, N.T. Aboulkhair, M. Simonelli, M. East, I.A. Ashcroft, R.J.M. Hague, From impact to solidification in drop-on-demand metal additive manufacturing using MetalJet, Addit. Manuf. 55 (Jul. 2022) 102827, https://doi.org/10.1016/J.ADDMA.2022.102827.

[15] V. Sukhotskiy, K. Tawil, E. Einarsson, Printability regimes of pure metals using contactless magnetohydrodynamic drop-on-demand actuation, Phys. Fluids 33 (5) (May 2021) 053303, https://doi.org/10.1063/5.0050354.

[16] M. Simonelli, et al., Towards digital metal additive manufacturing via high-temperature drop-on-demand jetting, Addit. Manuf. 30 (Dec. 2019), https://doi.org/10.1016/J.ADDMA.2019.100930.

[17] S. Yin *et al.*, "Cold spray additive manufacturing and repair: Fundamentals and applications," *Additive Manufacturing*, vol. 21. Elsevier B.V., pp. 628–650, May 01, 2018. doi: 10.1016/j.addma.2018.04.017.

[18] T. Hussain, D.G. Mccartney, P.H. Shipway, D. Zhang, Bonding Mechanisms in Cold Spraying: The Contributions of Metallurgical and Mechanical Components, J. Therm. Spray Technol. 18 (2009), https://doi.org/10.1007/s11666-009-9298-1.

[19] P.D. Ownby, J. Liu, Surface energy of liquid copper and single-crystal sapphire and the wetting behavior of copper on sapphire, J. Adhes. Sci. Technol. 2 (1) (1988) 255–269, https://doi.org/10.1163/156856188X00264.

[20] A. Shrestha, R. Asthana, T.K. Lacksonen, M. Singh, Synthesis and characterization of air-sintered Al 2O 3-bronze composites, J. Mater. Eng. Perform. 18 (8) (Nov. 2009) 1041–1045, https://doi.org/10.1007/S11665-008-9348-8/FIGURES/5.

[21] B. Zhao, R. Liu, N. Sheng, Y. Mahmoudi, C. Zhu, Copper−Alumina Capsules for High-Temperature Thermal Energy Storage, Cite This ACS Appl. Eng. Mater 2023 (2023) 1335–1342, https://doi.org/10.1021/acsaenm.3c00053.

[22] M. Diemer, A. Neubrand, K.P. Trumble, J. Rödel, Influence of Oxygen Partial Pressure and Oxygen Content on the Wettability in the Copper–Oxygen–Alumina System, J. Am. Ceram. Soc. 82 (10) (Oct. 1999) 2825–2832, https://doi.org/10.1111/J.1151-2916.1999.TB02163.X.

[23] U. m.b.,, et al., Current Issues and Problems in the Joining of Ceramic to Metal, IntechOpen (2016), https://doi.org/10.5772/64524.

[24] Y.L. Müller, L.P.H. Jeurgens, A. Antušek, V. Turlo, Atomistic Assessment of Melting Point Depression and Enhanced Interfacial Diffusion of Cu in Confinement with AlN, ACS Appl. Mater. Interfaces 14 (22) (Jun. 2022) 26099–26115, https://doi.org/10.1021/ACSAMI.2C01347/ASSET/IMAGES/MEDIUM/AM2C01347_M017.GIF.

[25] Y. Shi, W. Chen, L. Dong, H. Li, Y. Fu, Enhancing copper infiltration into alumina using spark plasma sintering to achieve high performance Al2O3/Cu composites, Ceram. Int. 44 (1) (Jan. 2018) 57–64, https://doi.org/10.1016/J.CERAMINT.2017.09.062.

[26] J. Lv, Y. Huang, R. Fu, Y. Ji, B. Wu, X. Liu, AlN/Cu composite ceramic substrate fabricated using a novel TiN/AgCuTi composite brazing alloy, J. Eur. Ceram. Soc. 40 (15) (Dec. 2020) 5332–5338, https://doi.org/10.1016/J.JEURCERAMSOC.2020.07.060.

[27] H. Yi, L. Qi, J. Luo, Y. Guo, S. Li, N. Li, Elimination of droplet rebound off soluble substrate in metal droplet deposition, Mater. Lett. 216 (Apr. 2018) 232–235, https://doi.org/10.1016/J.MATLET.2018.01.127.

[28] R. Berkhout, W. P. J. Classens, H. C. M. Van Genuchten, and E. V Kuznetsov, "Device for ejecting droplets of a fluid having a high temperature," U.S. Patent No. 8,444,028, May 21, 2013.

[29] N. Gilani, N.T. Aboulkhair, M. Simonelli, M. East, I. Ashcroft, R.J.M. Hague, Insights into drop-on-demand metal additive manufacturing through an integrated experimental and computational study, Addit. Manuf. 48 (Dec. 2021) 102402, https://doi.org/10.1016/J.ADDMA.2021.102402.

[30] J.R. Fanchi, "Measures of Rock-Fluid Interactions", in Shared Earth Modeling, Butterworth-Heinemann (2002) 108–132, https://doi.org/10.1016/B978-075067522-2/50007-0.

[31] L. Su, et al., A new strategy for eliminating bottom hole defects during aluminum droplet printing within a broad temperature range, J. Mater. Process. Technol. 319 (Oct. 2023) 118079, https://doi.org/10.1016/j.jmatprotec.2023.118079.

[32] M. Entezarian, R.A.L. Drew, Direct bonding of copper to aluminum nitride, Mater. Sci. Eng. A 212 (2) (Jul. 1996) 206–212, https://doi.org/10.1016/0921-5093(96)10190-8.

[33] N. Hayati-Roodbari, A. Wheeldon, C. Hendler, A. Fian, and R. Trattnig, "Ohmic contact formation for inkjet-printed nanoparticle copper inks on highly doped GaAs," *Nanotechnology*, vol. 32, no. 22, 2021, doi: 10.1088/1361-6528/abe902.

[34] Q. Mao, Y. Zhang, Y. Guo, Y. Zhao, Enhanced electrical conductivity and mechanical properties in thermally stable fine-grained copper wire, Commun Mater 2 (2021), https://doi.org/10.1038/s43246-021-00150-1.